

Article

Symurban Nanocrystals for Advanced Anti-Pollution Skincare

Daniel Köpke and Sung Min Pyo *

Department of Biology, Chemistry, Pharmacy, Free University of Berlin, 14195 Berlin, Germany; d.koepke@fu-berlin.de

* Correspondence: pyo.sungmin@fu-berlin.de; Tel.: +49-30-838 50703

Received: 19 February 2020; Accepted: 9 March 2020; Published: 11 March 2020



Abstract: Several of most common dermatoses worldwide, e.g., psoriasis and atopic dermatitis, are worsened in their clinical picture when the skin is regularly exposed to an increased air pollution level, e.g., particulate matter. This is explainable by the activation of the aryl hydrocarbon receptor (AhR) in the skin, which results in an increased release of proinflammatory cytokines and matrix metalloproteinases. Symurban is a competitive AhR antagonist and thus allows the effective protection of skin. In order to improve its dermal bioavailability as a poorly soluble active agent (0.25 µg/mL), nanocrystals were prepared and evaluated. Nanocrystals are pure active crystals reduced in particle size to the submicron range of 100 to 1000 nm. They feature the properties of nanocrystals, such as increased saturation solubility and dissolution velocity, without having to be declared as nanomaterial. Production methods and parameters were systematically investigated. Wet bead milling at 2000 rpm for 30 min yielded the best results. A z-average of 280 nm was achieved for a 10% Symurban suspension with a polydispersity index of 0.20, indicating a narrow size distribution. For the long-term stabilization of the nanocrystal suspension, the performance of 15 surfactants of different categories and HLB values were investigated and evaluated. It was found that non-ionic surfactants in general were better able to stabilize the system than anionic or amphoteric surfactants. Highest stability of over 12 months at 25 °C was achieved with 2% Plantacare 810 UP, an ECOCERT surfactant with high skin tolerance. The suspension was also chemically long-term stable with >97% of remaining Symurban over 12 months. The saturation solubility of Symurban as nanocrystals was significantly increased from 0.25 to 2.9 µg/mL, which corresponds to a factor of >11. In a case study of one male volunteer with healthy skin conditions, penetration profiles of Symurban nanocrystal hydrogel and commercial anti-pollution serum containing an identical amount of Symurban were determined and compared. After 20 min of exposure, the relative Symurban concentration in the deeper skin layers (tape 19-30) was more than two times higher for nanocrystal hydrogel (16%) than the commercial serum (7%). These results suggest that nanocrystals are a promising delivery system for the poorly soluble anti-pollution agent Symurban.

Keywords: benzylidene dimethoxydimethylindanone; competitive inhibitor of aryl hydrocarbon receptor; high pressure homogenization; wet bead milling; nanosuspension; gas chromatography–mass spectrometry; saturation solubility; skin penetration

1. Introduction

As a result of worldwide urbanization, the quality of air is constantly declining. According to the World Health Organization (WHO), 91% of urban population is exposed to air quality exceeding the limit of health concern [1]. A correlation between air quality and diseases affecting the lungs and cardiovascular systems has already been proven with 29% of lung cancer, 25% of heart diseases, and 43% of lung diseases attributed to air pollution in 2016 [1]. In recent years, increasingly the effect

of air pollution on the largest organ exposed to the environment, the skin, has been studied [2–4]. Air pollution is defined as the contamination of the environment by any agent that modifies the natural characteristics of the atmosphere. According to the WHO, pollutants of major public health concern include particulate matter, carbon monoxide, ozone, nitrogen dioxide and sulfur dioxide [1]. It was found that in particular, the exposure of the skin to polycyclic aromatic hydrocarbons (PAHs) and halogenated aromatic hydrocarbons (HAHs) is harmful. They originate from incomplete burning of organic material and are primarily present in industrial exhaust gases, fuel burning, cigarette smoke, etc., and are transported by airborne fine dust particles [5]. Penetrating into skin, the transcription factor aryl hydrocarbon receptor (AhR) is specifically activated [6–9], resulting in the upregulation of various pharmacological processes, e.g., enzymes of the cytochrome P450 family [10], melanogenesis [11], cellular oxidant/antioxidant regulation [12], immune regulation [13–15] and regulation of the epidermal barrier function [16] (Figure 1). From this, the pathogenesis of various skin diseases is stimulated, such as vitiligo [17], psoriasis [18,19] scleroderma [20], neurodermatitis [21], and acne vulgaris [22]. Further, the promotion of dermal carcinogenesis is discussed in following references [23–25].

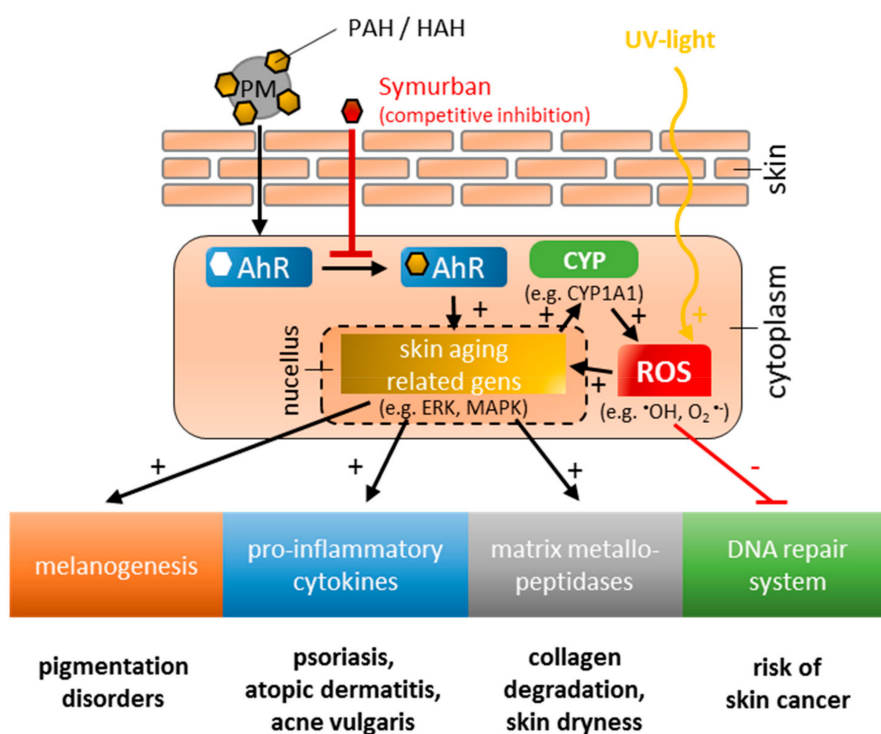


Figure 1. Schematic illustration of impacts on skin caused by polycyclic aromatic hydrocarbons (PAHs) and hydrogenated aromatic hydrocarbons (HAHs) adherent to the surface of particulate matter (PM), and UV-light exposure.

The concern about skin damage caused by air pollution is particularly evident in the personal care segment, where in 2016, 79% of all products marketed worldwide had an anti-pollution claim [26]. In the same year, Symurban (INCI: Benzylidene Dimethoxydimethylindanone) was introduced to the market by the company Symrise as an anti-pollution active agent. As a competitive inhibitor of AhR, Symurban inhibits PAH/HAH-induced effects [27–29]. However, its low solubility results in low penetration. One physical approach for increasing its saturation solubility and thereby its dermal bioavailability is the formation of nanocrystals [30–34]. By the reduction of particle size from the μm -range to the nm-range, a significantly increased saturation solubility [34–37] and a higher dissolution rate [30,37,38] can be achieved. As a result, a greater concentration gradient is created between the formulation and the skin, enhancing the passive diffusion of the active ingredient into the skin. Due to the increased dissolution rate, the penetrated active agent molecules can then be quickly

replaced, and the high concentration gradient can be maintained over a long period of time. To avoid consumer concerns about nanoproducts, the size of the particles can be adjusted to the so-called submicron range of 100–1000 nm. They still have the properties of nanocrystals, but do not have to be declared as nanomaterials, since according to the EU regulation, a product only has to be labelled as nano if more than 50% of the particles have a diameter of <100 nm [39].

Therefore, the aim of this work was to apply nanocrystal technology on Symurban to increase its solubility and thereby its skin penetration in order to obtain the full potency of Symurban as an anti-pollution agent *in vivo*.

2. Materials and Methods

2.1. Materials

All materials used in this work are listed in Table 1, including trade name, INCI name and manufacturer/distributor. Milli-Q water was freshly produced using a Milli-Q system from Millipore GmbH (Darmstadt, Germany).

Table 1. Overview of all materials used in this work.

	Trade Name	INCI/Chemical Description	Manufacturer/Distributor
active	Symurban®	Benzylidene Dimethoxydimethylindanone	Symrise AG, Germany
	Amphoterge® W-2	Disodium Cocoamphoacetate	Lonza Group AG, Switzerland
surfactants	Bergasoft SCG 22	Sodium Cocoyl Glycinate	Berg + Schmidt GmbH & Co. KG, Germany
	Dermofeel® G10L	Polyglyceryl-10 Laurate	Evonik Dr. Straetmans GmbH, Germany
	Eumulgin® SG	Sodium Stearoyl Glutamate	BASF SE, Germany
	Kolliphor® P407	Poloxamer 407	BASF SE, Germany
	Lanette® E	Cetaryl sulphate	BASF SE, Germany
	Miranol® Ultra C32	Sodium Cocoamphoacetate	Solvay, Belgium
	Plantacare® 2000 UP	Decyl-Glucoside	BASF SE, Germany
	Plantacare® 810 UP	Coco-Glucoside	BASF SE, Germany
	Polyaldo® 10-1-CC	Polyglyceryl-10 Caprylate/Caprates	Lonza Group AG, Switzerland
	Sisterna® L70-C	Sucrose Alkyl Ester	Sisterna B.V., Netherlands
	Sisterna® SP70-C	Sucrose Alkyl Ester	Sisterna B.V., Netherlands
	SDS	Sodium Dodecyl Sulphate	VWR International LLC, USA
	Polysorbate 80	Polysorbate-80	Caesar & Loretz GmbH, Germany
others	Microcare® PEHG (preservative)	Phenoxyethanol and Ethylhexylglycerin	Dr. Rimpler GmbH, Germany
	Carbopol® 981 NF (gelling agent)	Carbomer	Lubrizol Advanced Materials Europe BVBA, Belgium
GC materials	tert-Butyl methyl ether, HPLC grade, 99%+	Methyl tert-butyl ether 99%+	ThermoFischer (Kandel) GmbH, Germany
	Alphagaz™ 1 He	Helium 99,999%	AIR LIQUIDE Deutschland GmbH, Germany

2.2. Production of Symurban Nanocrystals

2.2.1. High-Pressure Homogenization

Symurban (10 wt%), Polysorbate 80 (2 wt%) and double-distilled water (88 wt%) were pre-homogenized using a rotor-stator-homogenizer (Ultra-Turrax T25, IKA-Werke GmbH & Co. KG, Staufen im Breisgau, Germany) at 8500 rpm for 60 seconds. The obtained pre-suspension was subsequently high-pressure homogenized (Micron LAB 40, APV Gaulin GmbH, Langenhagen, Germany) in 3 steps—2 cycles at 500 bar, 2 cycles at 1000 bar and 15 cycles at 1500 bar. High-pressure homogenization is a high-energy process that leads to a temperature increase of the sample above room temperature during production. When the sample cools down to room temperature again after production, the system is supersaturated and Ostwald ripening occurs. To avoid this, the production temperature was set to 5 °C.

2.2.2. Bead Milling

Symurban (10 wt%), Polysorbate 80 (2 wt%) and double-distilled water (88 wt%) were milled in a PML-2 pearl mill (Bühler AG, Uzwil, Switzerland) using SiLibeads type ZY-E 0.4–0.6 mm (Sigmund Lindner GmbH, Warmensteinach, Germany). Milling time was set to 30 min, the rotation speed to 2000 rpm and the temperature, here also, at 5 °C. After comparing both methods for their suitability to produce Symurban nanocrystals using the surfactant Polysorbate 80 as standard, a detailed surfactant screening (c.f. Table 1 of Section 2.1.) was subsequently carried out on the bead mill. Therefore, Symurban (10 wt%), on 15 selected surfactants (2 wt%) and double-distilled water (88 wt%), was milled for 20 min at a rotation speed of 2000 rpm and 5 °C.

2.3. Particle Characterization

2.3.1. Photon Correlation Spectroscopy (PCS)

The mean particle diameter and polydispersity index (PDI) of prepared nanocrystals were determined by dynamic light scattering using a Zetasizer Nano ZS (Malvern Instruments, Worcestershire, UK). Before measurement, the samples were diluted 1:1000 (vol%) in Milli-Q-water. Each sample was measured 10 times and the average was calculated and reported as a z-average (z-ave).

2.3.2. Laser Diffraction (LD)

The volume-weighted particle diameter and distribution were measured by laser diffraction using a Mastersizer 2000 equipped with a Hydro 2000S dispersing unit (both Malvern Instruments, Worcestershire, UK). The refractive index used for Symurban was 1.610, which was determined prior to LD measurement. As imaginary refractive index 0.100 was used. Sample was added to the dispersion unit until a laser obscuration between 4–6% was reached. Stirring speed was set to 1750 rpm. Loose aggregates, if present, were re-dispersed by ultrasound at 25% to 75%.

2.3.3. Light Microscopy

Samples were additionally examined by light microscopy using BA 210 (Motic Deutschland GmbH, Wetzlar, Germany) at 100-, 400-, and 1000-times magnification to detect possible particles and aggregates in μm -size.

2.3.4. Zeta Potential

The surface charge of prepared nanocrystals was determined using the Zetasizer Nano ZS again (c.f. 2.3.1). Prior to measurement, the sample was diluted 1:100 (vol%) with conductivity-adjusted water (to 50 $\mu\text{S}/\text{cm}$ with NaCl) at 20 °C. One sample was measured in triplicate and the calculated mean value was used as the result.

2.4. Gas Chromatography–Mass Spectrometry (GC-MS)

The Symurban concentration was determined to assess the chemical stability, saturation solubility and the penetration of Symurban nanocrystals. Therefore, GC-MS analysis was carried out using an Agilent Technologies 7890A GC System paired with an Agilent Technologies 5975C quadrupole MS-detector. As a column, an Agilent J&W GC column type 122–5532 G was used. At a heating rate of 20 K/min, the temperature was raised from 120 to 320 °C and maintained for 5 min. The flow rate of helium in the mobile phase was set to 1 mL/min. For the measurement, 2 µL of sample was injected with a split ratio of 1:10. The detector was used in SIM-mode at a molar mass of 293 M, being the main peak of mono-demethylated Symurban derivative, formed due to electron impact ionization. Symurban as the E and Z isomer was detected at the retention times of 11.6 and 11.8 min, respectively. The total amount of Symurban was calculated as the sum of the two peaks. Each measurement was performed in duplicate and averaged. The method was calibrated by a 2nd degree polynomial regression curve with a coefficient of determination of 0.9969. The limit of quantification was determined to be 0.25 µg/mL.

2.5. Determination of Saturation Solubility

For the investigation of saturation solubility, nanocrystal suspension was diluted in Milli-Q-water to a Symurban concentration of 1.0%. As reference, 1.0% Symurban raw drug powder was dispersed in 0.4% aqueous Plantacare 810 UP solution to keep the surfactant concentration equal to the dilution of nanocrystals. Both dilutions were then shaken for 24 h in an Innova 4230 shaker (New Brunswick Scientific GmbH, Nürtingen, Germany) at 25 °C and 150 rpm. The undissolved Symurban crystals were removed by filtration using a 25 mm Cellulose Nitrate syringe-filter with a cutoff of 0.1 µm (GE Helathcare Life Sciences, Buckinghamshire, UK). Filtrates were diluted immediately 1:2 in aqueous 0.4% Plantacare 810 UP solution to avoid re-crystallization of supersaturated solution. Symurban concentration was then measured by GC-MS, c.f. Section 2.4. The determination of saturation solubility was done in triplicate. A Tuckey test was performed to determine significance ($p < 0.01$).

2.6. Skin Penetration Study

The skin penetration of Symurban nanocrystals was determined in a case study on one male volunteer using the tape stripping method [40,41]. The volunteer obtained written information about the purpose, extent, potential risks and the aim of the study. In addition, an informational conversation was held in which the volunteer was able to ask open questions. His willingness to participate in this study was confirmed by his signature, as well as the information that the willingness can be countermanded at any time without any personal disadvantage. Symurban nanocrystal hydrogel at 0.25% was prepared using Carbopol 981 NF at 0.25% as gelling agent. On the inner forearm of the volunteer, an area of 1.5 × 2 cm was treated with 45 mg of prepared hydrogel. After 20 min, the area was tape stripped 30 times using tesafilm® Kristallklar (tesa SE, Norderstedt, Hamburg, Germany). The Symurban removed by the adhesive tapes was extracted in 3.5 mL methyl tert-butyl ether and the concentration in supernatant analyzed by GC-MS, c.f. Section 2.4. As a reference formulation, a high-quality anti-pollution facial serum with 0.25% Symurban (measured by GC-MS) and comparable viscosity to nanocrystal hydrogel was used.

3. Results and Discussion

3.1. Production Method of Symurban Nanocrystals

For the production of Symurban nanocrystals, the two commonly applied top-down methods, high pressure homogenization and bead milling, were used. An aqueous Symurban suspension at 10% was prepared and processed, stabilized by 2.0% Polysorbate 80 for stabilizing nanosized suspensions. Unprocessed Symurban raw drug powder had a broad size distribution (0.4 to 800 µm) with a peak maximum at 25 µm (Figure 2, red curve). Applying five cycles of high-pressure homogenization at 1500 bar considerably decreased both the width of distribution (0.4 to 40 µm) and the peak maximum to

5.4 μm . However, after 10 cycles, almost no change in size distribution and peak maximum was observed. Even after a total of 15 homogenization cycles, the peak maximum decreased only marginally to 4.1 μm (Figure 2, light-blue curve) and the desired nm range was not reached. Therefore, high-pressure homogenization was considered to be unsuited for the production of Symurban nanocrystals.

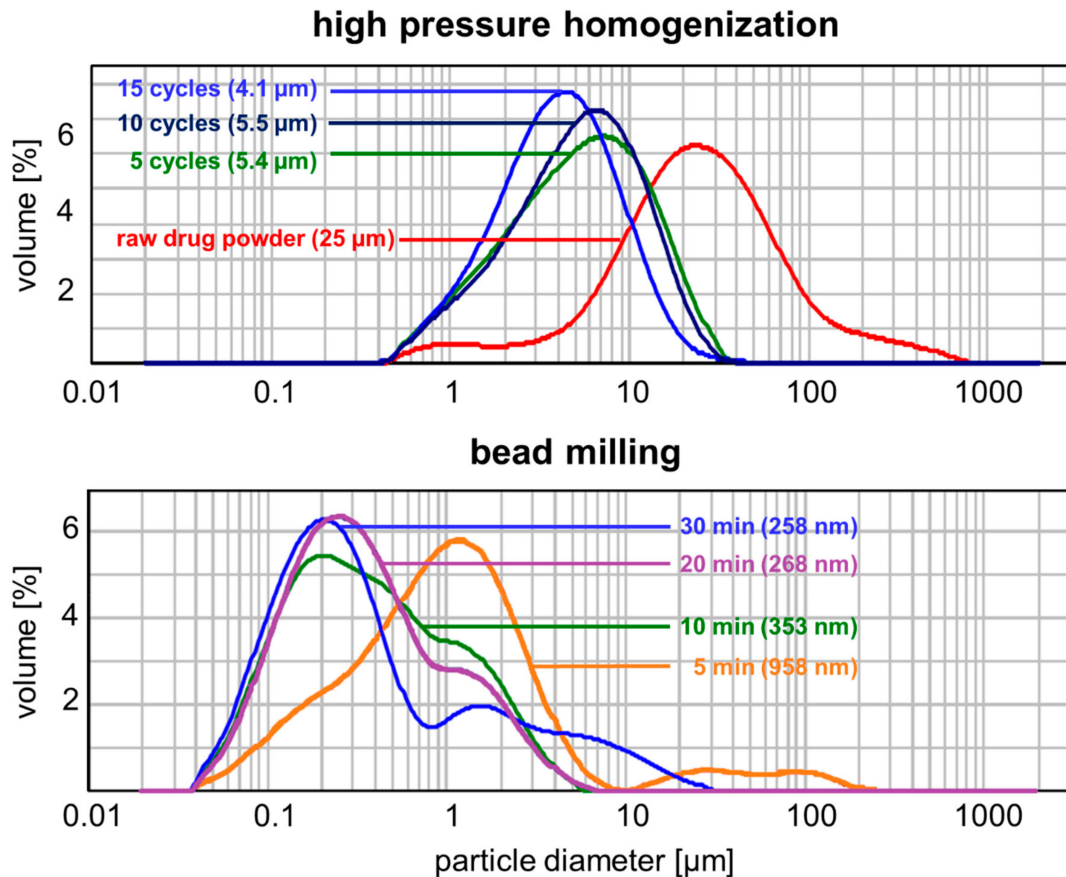


Figure 2. Laser diffraction (LD) particle size distribution of Symurban nanocrystals produced by high-pressure homogenization (upper) and bead milling (lower), showing that only bead milling leads to appropriate size reduction of Symurban μm -crystals.

Besides the high-pressure homogenization, bead milling was also examined for its suitability to produce Symurban nanocrystals. Already after a milling time of 5 min, the peak maximum of the raw drug powder curve at 25 μm shifted to 0.95 μm , being in the targeted nm-range. The particle size distribution was still broad, with the presence of a second particle fraction with sizes of 10–200 μm . This can be attributed to an unground fraction of the sample. After 20 min of milling, the second fraction $>10 \mu\text{m}$ completely disappeared and the peak maximum shifted to 268 nm. The increase of the milling time to 30 min leads to a so-called “over-processing” of the suspension, visible in the further broadening of the particle distribution from 0.04 to 7 μm (20 min) to 0.04–30 μm (30 min). A narrow distribution is, however, essential for nanocrystal suspensions, as storage stability is considerably higher than for broad-distributed suspensions whose small particles dissolve in favour of the large particles (Ostwald ripening, [42]).

In conclusion, Symurban nanocrystals at 10% can be obtained by bead milling. Optimal milling time was determined to be 20 min. Stabilized by Polysorbate 80 at 2.0% PCS, a z-ave of 295 nm with polydispersity index of 0.32 was achieved. These values were in good agreement with LD diameters LD50% of 0.26 μm , LD90% of 1.74 μm , and LD95% of 2.81 μm .

3.2. Screening of Surfactants

A selection of 15 surfactants from different types (anionic, amphoteric, non-ionic-PEG, non-ionic-polyglyceryl and non-ionic-glucoside) was used at 2.0% to stabilize 10.0% Symurban nanocrystal suspensions. The majority of the surfactants tested are ECOCERT-certified and are highlighted in green in Figure 3. In addition, four surfactants were tested, which are not ECOCERT-certified but have excellent stabilizing properties. These surfactants are highlighted in red in Figure 3. Directly after production, all suspensions were examined under the microscope. Respective images are shown in Figure 3 with their corresponding LD50% values (Figure 3, left), zeta potentials (Figure 3, middle) and PCS z-averages (Figure 3, right). Six of fifteen surfactants, i.e., Bergasoft SCG 22, Eumulgin SG, Lanette E, Miranol Ultra C32, SDS and Sisterna SP70-C, showed a pronounced tendency to form large aggregates visible to the naked eye already on the day of production. For these samples, particle size and zeta potential were not determined (abbreviated as n.d. in Figure 3).

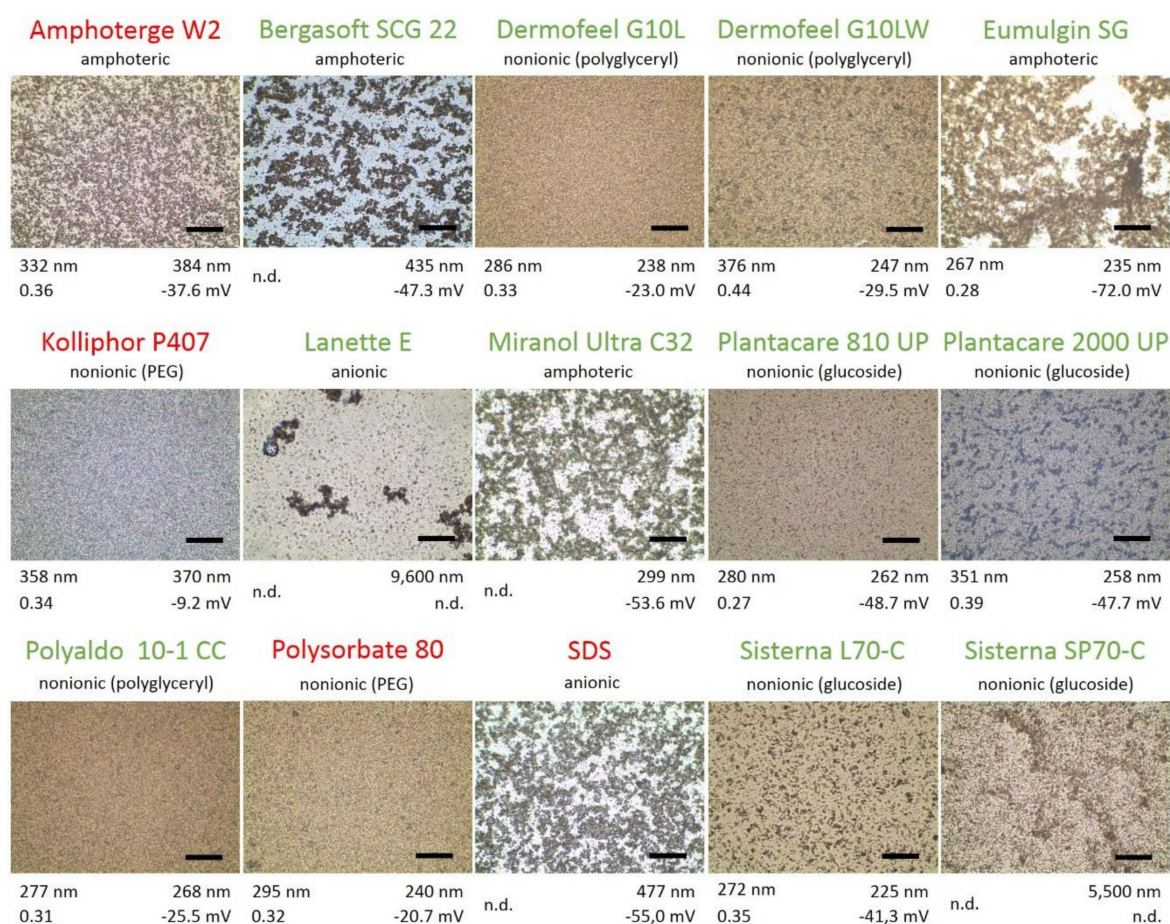


Figure 3. Microscopic images at 400-fold magnification (scale bar 50 μm) for all produced samples with 2% surfactant, where ECOCERT surfactants are highlighted green and non-ECOCERT surfactants in red. The type of surfactant used is written above respective image, the z-average (z-ave) and polydispersity index (PDI) left under the image, and LD50% value and zeta potential right under the image.

Clear tendencies could be identified in the surfactant screening. With anionic and amphoteric surfactants, no stable Symurban nanocrystal suspension could be obtained, with all showing a pronounced formation of aggregates. Furthermore, surfactants with high hydrophilic properties indicated by high HLB values >20 proved to be unsuited for Symurban nanocrystal stabilization. Among the three subtypes of non-ionic surfactants, PEG, polyglyceryl and glucoside, no correlation could be found. In each of the three subtype groups, both representatives can be found, one with high stabilizing properties in terms of particle size and size distribution and one showing pronounced aggregation

(e.g., Plantacare 2000 UP led to aggregation whereas Plantacare 810 UP remained stable—both are alkyl glucosides).

The four best-performing surfactants among the 15 surfactants tested in terms of appearance (no aggregates), particle size (PCS mean particle size < 300 nm, LD50% < 300 nm), and size distribution (PdI < 0.35) were identified as Dermofeel G10L, Plantacare 810 UP, Polyaldo 10-1-CC, and Sisterna L70-C.

3.3. Storage Stability of Symurban Nanocrystals

The four best formulations were stored in the refrigerator at 4 °C, at 25 °C and in the oven at 40 °C, and their physical stability was re-analyzed after 1 month. After 1 month of storage of Dermofeel G10L stabilized formulation at 25 °C, mean particle size and PdI clearly increased from 286 to 598 nm and from 0.33 to 0.45 (Table 2). The LD90% value > 1.3 µm additionally confirmed that this formulation is not storage-stable. Comparable observations were made for the Sisterna L70-C-stabilized formulation. With a z-ave of 522 nm, PdI of 0.5 and LD90% > 4 µm at the same storage conditions, this formulation was not stable.

Table 2. Particle size (PCS z-ave, LD D50, D90 and D95 all in [nm]) and polydispersity index (PdI) of Symurban nanocrystals produced with 1.5% of the 4 best surfactants after 1 month storage at 4, 25, and 40 °C, showing that Plantacare 810 UP provides the highest physical storage stability. Values exceeding the nm-range were written in red.

Surfactant	1 Month at 4 °C					1 Month at 25 °C					1 Month at 40 °C				
	z-ave	PdI	D50	D90	D95	z-ave	PdI	D50	D90	D95	z-ave	PdI	D50	D90	D95
Dermofeel G10L	307	0.30	252	799	1085	598	0.45	307	1332	1674	747	0.31	1175	3042	4368
Plantacare 810 UP	263	0.20	257	569	708	270	0.21	231	449	523	345	0.20	295	758	3342
Polyaldo 10-1-CC	286	0.20	249	622	815	357	0.24	315	1206	1988	532	0.28	428	3371	27,401
Sisterna L70-C	263	0.34	268	2454	3243	522	0.50	2028	4353	5191	1589	0.58	2448	4767	5780

In contrast, Plantacare 810 UP and the Polyaldo 10-1-CC-stabilized formulation showed no noticeable changes under the microscope after 1 month storage at 25 °C. Both z-ave and PdI remained stable below 360 nm and 0.24, respectively. The only difference between the two was the LD95% and LD99% values. A higher storage stability was observed for the Plantacare 810 UP sample with an LD99% value of < 1 µm versus > 4 µm for the Polyaldo-10-1-CC sample. Furthermore, at the two other storage temperatures of 4 and 40 °C, the Plantacare 810 UP formulation was superior with smaller z-ave, PdI and LD99% values. Both are non-ionic surfactants sterically stabilizing the particles in the suspension. However, in contrast to the Polyaldo-10-1-CC formulation, the Plantacare 810 UP formulation provides additional electrostatic stabilization based on the low zeta potential of −49 mV. This may explain the higher storage stability of the Plantacare 810 UP formulation. For this formulation, sufficient stability over 1 year was demonstrated at 25 °C, with a z-ave of 354 nm, a PdI of 0.20 and an LD95% value of <1 µm (Figure 4). The formulation also showed sufficient stability at 4 °C storage. Under stress conditions of 40 °C, crystal growth was observed. This can be explained by increased solubility and decreased viscosity of the formulation at higher temperatures, promoting Ostwald ripening.

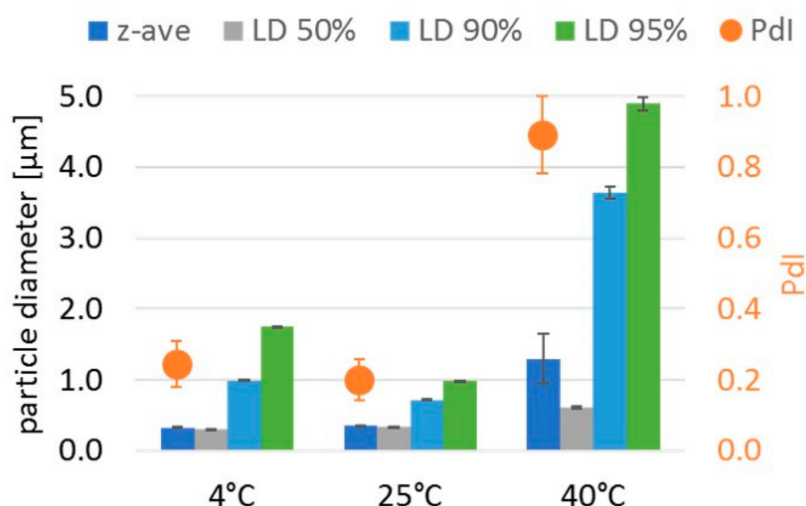


Figure 4. Particle size and polydispersity index of Symurban nanocrystals stabilized with 2% Plantacare 810 UP after 12 months of storage at 4, 25 and 40 °C. Best stability was achieved at 25 °C followed by 4 °C. Under stress conditions of 40 °C, aggregation occurred.

In conclusion, Symurban nanocrystals at 10% stabilized with the ECOCERT-certified Plantacare 810 UP at 2.0% proved to be storage-stable for 1 year at both 4 and 25 °C.

Furthermore, the formulation proofed to be chemically stable. After 1 year of storage, no significant reduction of Symurban concentration as nanocrystal suspensions was observed at any storage temperature (4, 25 and 40 °C) with the minimum remaining Symurban content of $>97.5 \pm 0.21\%$.

All in all, the best formulation, consisting of 10% Symurban, 2% Plantacare 810 UP and 88% Milli-Q water and produced by 20 min of wet bead milling, proved to be highly stable physically and chemically. The recommended storage temperature was found to be 25 °C, but a storage at 4 °C also proved to be feasible.

3.4. Saturation Solubility

The increased dermal bioavailability of active compounds by nanocrystal technology is achieved through increased saturation solubility. Therefore, the extent of saturation solubility increase of Symurban as nanocrystals is of interest. It was measured by GC (c.f. 2.4.) and compared to unprocessed μm -sized raw drug powder in water and in 0.2% aqueous Plantacare 810 UP solution (identical to the composition of nanocrystal suspension). Results of the saturation solubility study are presented in Figure 5. The saturation solubility for the nanocrystal formulation is significantly increased by a factor of >15 for raw drug powder in an aqueous surfactant solution and > 11 for raw drug powder in water from $0.19 \pm 0.05 \mu\text{g/mL}$ and $0.25 \pm 0.02 \mu\text{g/mL}$ to $2.86 \pm 0.45 \mu\text{g/mL}$, respectively. As the penetration of active compounds into skin is a passive diffusion process, it is mainly dependent on the concentration gradient between the formulation and skin and therefore on the saturation concentration of active compounds in the formulation [30,33,34]. By preparing Symurban as nanocrystals, a clearly improved dermal bioavailability can therefore be expected.

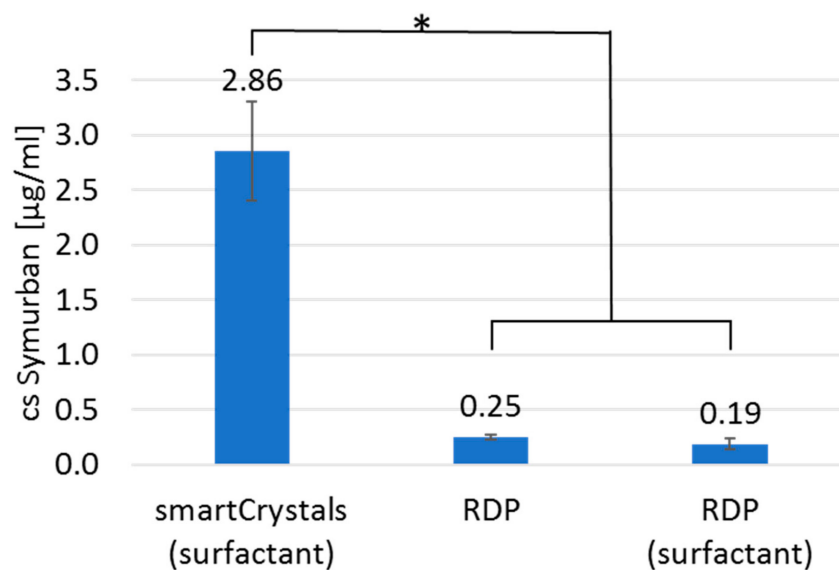


Figure 5. Saturation solubility of Symurban as nanocrystals and raw drug powder (RDP) in water and in aqueous surfactant solution according to the composition of nanocrystal suspension, demonstrating at least an 11-fold increased saturation solubility by nanocrystal technology.

3.5. Skin Penetration Profile

The assumption of improved dermal bioavailability by increased saturation solubility was verified in a case study on a male volunteer using the tape stripping method. Instead of using a hydrogel with Symurban μ m-crystals as a reference, the performance of nanocrystal hydrogel was compared to a Symurban-containing market product of higher price level with an anti-pollution claim. The selection of a product being already optimized for the market was intended to challenge the nanocrystals as delivery system.

Both formulations had the same Symurban content of 0.25 wt%. Furthermore, the applied amount of formulation and size of skin area were kept identical. After 20 min of penetration, each skin area was taped 30 times and the content of Symurban in the tapes was determined via GC (c.f. 2.4.) to create penetration profiles. The recovery rate of both formulations was comparable with 90.2% (reference product) and 92.3% (smartCyrstals gel). The loss of <10% is attributable to the fact that active ingredients penetrate not only vertically but also horizontally. The penetration depth exceeded the depth reached by 30 tapes and could therefore not be determined and compared. Clear differences can be seen in the distribution of the active ingredient in the skin (Figure 6). The penetration profile of market product shows that 47% and therefore almost half of applied Symurban are located in the first 2 tapes (Figure 6, grey bars). With 7% in the tapes 19-30, only a negligible amount reaches the deeper layers. In contrast, the nanocrystal hydrogel allowed deeper penetration of larger amounts of Symurban, which is reflected in the Symurban content of only 26% in the first two tapes and more than twice as much in tapes 19-30 (Figure 6, yellow bars). Symurban nanocrystal hydrogel therefore shows a more favorable distribution, with higher concentrations in the deeper layers of the stratum corneum.

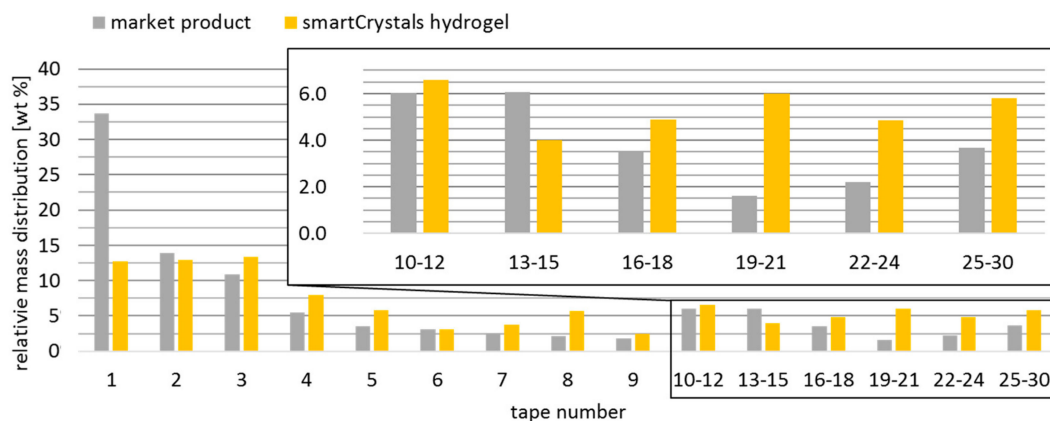


Figure 6. Penetration profiles measured on the inner forearm of one volunteer with healthy skin conditions via a tape stripping test after 20 min application of Symurban nanocrystal hydrogel (yellow bars) and a commercially available anti-pollution product (grey bars) with identical Symurban amount.

The present data confirm that by reducing the crystal size of Symurban into the submicron range, its penetration can be improved. This result is consistent with data from literature showing superior skin penetration of submicron particles compared to raw drug powder [30–34].

4. Conclusions

A Symurban nanocrystal suspension at 10 wt% with mean particle size of 280 nm and PDI of 0.27 was obtained by wet bead milling at 2000 rpm for 30 min. Generally, Symurban nanocrystals were better stabilized by non-ionic surfactants compared to anionic surfactants. Highest physical and chemical storage stability among the 15 screened surfactants was obtained with 2 wt% Plantacare 810 UP, a skin-friendly and organic-certified surfactant. No particle growth (z-ave of 354 nm and PDI of 0.20) nor chemical degradation (>97%) was observed within 12 months at 4 °C and at room temperature. By nanocrystal technology, an increase in saturation solubility by a factor of >11 was obtained, leading to a favorable penetration profile with higher concentration of Symurban in deeper skin layers demonstrated by a tape stripping test on the inner forearm of one volunteer. Thus, nanocrystals can be seen as a highly promising system of poorly soluble Symurban to provide a more effective protection of the skin from harmful environmental pollution.

Author Contributions: Conceptualization, D.K. and S.M.P.; methodology, D.K. and S.M.P.; validation, D.K. and S.M.P.; formal analysis, S.M.P.; investigation, D.K. and S.M.P.; data curation, D.K. and S.M.P.; writing—original draft preparation, S.M.P.; writing—review and editing, D.K. and S.M.P.; visualization, D.K. and S.M.P.; supervision, S.M.P.; project administration, S.M.P. All authors have read and agreed to the published version of the manuscript.

Funding: This research received no external funding.

Conflicts of Interest: The authors declare no conflict of interest.

References

1. WHO. World Health Organization International Website. Available online: <https://www.who.int/airpollution/en/> (accessed on 21 October 2019).
2. Kim, K.E.; Cho, D.; Park, H.J. Air pollution and skin diseases: Adverse effects of airborne particulate matter on various skin diseases. *Life Sci.* **2016**, *152*, 126–134. [CrossRef] [PubMed]
3. Puri, P.; Nandar, S.K.; Kathuria, S.; Ramesh, V. Effects of air pollution on the skin: A review. *Indian J. Dermatol. Venereol. Leprol.* **2017**, *83*, 415–423. [CrossRef] [PubMed]
4. Mancebo, S.E.; Wang, S.Q. Recognizing the impact of ambient air pollution on skin health. *J. Eur. Acad. Dermatol. Venereol.* **2015**, *29*, 2326–2332. [CrossRef] [PubMed]

5. Alomirah, H.; Al-Zenki, S.; Al-Hooti, S.; Zaghoul, S.; Sawaya, W.; Ahmed, N.; Kannan, K. Concentrations and dietary exposure to polycyclic aromatic hydrocarbons (PAHs) from grilled and smoked foods. *Food Control* **2011**, *22*, 2028–2035. [[CrossRef](#)]
6. Denison, M.S.; Heath-Pagliuso, S. The Ah receptor: A regulator of the biochemical and toxicological actions of structurally diverse chemicals. *Bull. Environ. Contam. Toxicol.* **1998**, *61*, 557–568. [[CrossRef](#)] [[PubMed](#)]
7. Denison, M.S.; Nagy, S.R. Activation of the aryl hydrocarbon receptor by structurally diverse exogenous and endogenous chemicals. *Annu. Rev. Pharmacol. Toxicol.* **2003**, *43*, 309–334. [[CrossRef](#)]
8. Hankinson, O. The aryl hydrocarbon receptor complex. *Annu. Rev. Pharmacol. Toxicol.* **1995**, *35*, 307–340. [[CrossRef](#)]
9. Marlowe, J.L.; Puga, A. Aryl hydrocarbon receptor, cell cycle regulation, toxicity, and tumorigenesis. *J. Cell. Biochem.* **2005**, *96*, 1174–1184. [[CrossRef](#)]
10. Fujii-Kuriyama, Y.; Mimura, J. Molecular mechanisms of AhR functions in the regulation of cytochrome P450 genes. *Biochem. Biophys. Res. Commun.* **2005**, *338*, 311–317. [[CrossRef](#)]
11. Luecke, S.; Backlund, M.; Jux, B.; Esser, C.; Krutmann, J.; Rannug, A. The aryl hydrocarbon receptor (AHR), a novel regulator of human melanogenesis. *Pigment Cell Melanoma Res.* **2010**, *23*, 828–833. [[CrossRef](#)]
12. Dietrich, C. Antioxidant Functions of the Aryl Hydrocarbon Receptor. *Stem Cells Int.* **2016**. [[CrossRef](#)] [[PubMed](#)]
13. Esser, C.; Rannug, A.; Stockinger, B. The aryl hydrocarbon receptor in immunity. *Trends Immunol.* **2009**, *30*, 447–454. [[CrossRef](#)] [[PubMed](#)]
14. Stockinger, B.; Di Meglio, P.; Gialitakis, M.; Duarte, J.H. The aryl hydrocarbon receptor: Multitasking in the immune system. *Annu. Rev. Immunol.* **2014**, *32*, 403–432. [[CrossRef](#)] [[PubMed](#)]
15. Veldhoen, M.; Hirota, K.; Westendorf, A.M.; Buer, J.; Dumoutier, L.; Renaud, J.-C.; Stockinger, B. The aryl hydrocarbon receptor links T_H17-cell-mediated autoimmunity to environmental toxins. *Nature* **2008**, *453*, 106. [[CrossRef](#)] [[PubMed](#)]
16. Haas, K.; Weighardt, H.; Deenen, R.; Köhrer, K.; Clausen, B.; Zahner, S.; Boukamp, P.; Bloch, W.; Krutmann, J.; Esser, C. Aryl Hydrocarbon Receptor in Keratinocytes Is Essential for Murine Skin Barrier Integrity. *J. Investig. Dermatol.* **2016**, *136*, 2260–2269. [[CrossRef](#)]
17. Behfarjam, F.; Jadali, Z. Vitiligo patients show significant up-regulation of aryl hydrocarbon receptor transcription factor. *An. Bras. Dermatol.* **2018**, *93*, 302–303. [[CrossRef](#)]
18. Beránek, M.; Fiala, Z.; Kremláček, J.; Andrýs, C.; Krejsek, J.; Hamáková, K.; Palička, V.; Borská, L. Serum Levels of Aryl Hydrocarbon Receptor, Cytochromes P450 1A1 and 1B1 in Patients with Exacerbated Psoriasis Vulgaris. *Folia Biol.* **2018**, *64*, 97–102.
19. Kim, H.O.; Kim, J.H.; Chung, B.Y.; Choi, M.G.; Park, C.W. Increased expression of the aryl hydrocarbon receptor in patients with chronic inflammatory skin diseases. *Exp. Dermatol.* **2014**, *23*, 278–281. [[CrossRef](#)]
20. Noakes, R. Dissecting the enigma of scleroderma: Possible involvement of the kynurenine pathway. *Pteridines* **2017**, *28*, 3172. [[CrossRef](#)]
21. Hidaka, T.; Ogawa, E.; Kobayashi, E.H.; Suzuki, T.; Funayama, R.; Nagashima, T.; Fujimura, T.; Aiba, S.; Nakayama, K.; Okuyama, R.; et al. The aryl hydrocarbon receptor AhR links atopic dermatitis and air pollution via induction of the neurotrophic factor artemin. *Nat. Immunol.* **2017**, *18*, 64. [[CrossRef](#)]
22. Fabbrocini, G.; Kaya, G.; Caseiro Silverio, P.; de Vita, V.; Kaya, A.; Fontao, F.; Sorg, O.; Saurat, J.-H. Aryl Hydrocarbon Receptor Activation in Acne Vulgaris Skin: A Case Series from the Region of Naples, Italy. *Dermatology* **2015**, *231*, 334–338. [[CrossRef](#)] [[PubMed](#)]
23. Kolluri, S.K.; Jin, U.-H.; Safe, S. Role of the aryl hydrocarbon receptor in carcinogenesis and potential as an anti-cancer drug target. *Arch. Toxicol.* **2017**, *91*, 2497–2513. [[CrossRef](#)] [[PubMed](#)]
24. Matsumoto, Y.; Ide, F.; Kishi, R.; Akutagawa, T.; Sakai, S.; Nakamura, M.; Ishikawa, T.; Fujii-Kuriyama, Y.; Nakatsuru, Y. Aryl Hydrocarbon Receptor Plays a Significant Role in Mediating Airborne Particulate-Induced Carcinogenesis in Mice. *Environ. Sci. Technol.* **2007**, *41*, 3775–3780. [[CrossRef](#)] [[PubMed](#)]
25. Xue, P.; Fu, J.; Zhou, Y. The Aryl Hydrocarbon Receptor and Tumor Immunity. *Front. Immunol.* **2018**, *9*, 286. [[CrossRef](#)] [[PubMed](#)]
26. Mistry, N. Guidelines for Formulating Anti-Pollution Products. *Cosmetics* **2017**, *4*, 57. [[CrossRef](#)]
27. Haarmann-Stemmann, T.; Esser, C.; Krutmann, J. The Janus-Faced Role of Aryl Hydrocarbon Receptor Signaling in the Skin: Consequences for Prevention and Treatment of Skin Disorders. *J. Investig. Dermatol.* **2015**, *135*, 2572–2576. [[CrossRef](#)]

28. Qiao, Y.; Li, Q.; Du, H.-Y.; Wang, Q.-W.; Huang, Y.; Liu, W. Airborne polycyclic aromatic hydrocarbons trigger human skin cells aging through aryl hydrocarbon receptor. *Biochem. Biophys. Res. Commun.* **2017**, *488*, 445–452. [[CrossRef](#)]
29. Tigges, J.; Haarmann-Stemmann, T.; Vogel, C.F.A.; Grindel, A.; Hübenthal, U.; Brenden, H.; Grether-Beck, S.; Vielhaber, G.; Johncock, W.; Krutmman, J.; et al. The new aryl hydrocarbon receptor antagonist E/Z-2-benzylindene-5,6-dimethoxy-3,3-dimethylindan-1-one protects against UVB-induced signal transduction. *J. Investig. Dermatol.* **2014**, *134*, 556–559. [[CrossRef](#)]
30. Hatahet, T.; Morille, M.; Hommoss, A.; Dorandeu, C.; Müller, R.H.; Bégu, S. Dermal quercetin nanocrystals®: Formulation development, antioxidant activity and cellular safety. *Eur. J. Pharm. Biopharm.* **2016**, *102*, 51–63. [[CrossRef](#)]
31. Pyo, S.; Meinke, M.; Keck, C.; Müller, R. Rutin—Increased Antioxidant Activity and Skin Penetration by Nanocrystal Technology (nanocrystals). *Cosmetics* **2016**, *3*, 9. [[CrossRef](#)]
32. Al Shaal, L.; Müller, R.H.; Shegokar, R. smartCrystal combination technology: Scale up from lab to pilot scale and long term stability. *Pharmazie* **2010**, *65*, 877–884. [[CrossRef](#)] [[PubMed](#)]
33. Pelikh, O.; Stahr, P.-L.; Huang, J.; Gerst, M.; Scholz, P.; Dietrich, H.; Geisel, N.; Keck, C.M. Nanocrystals for improved dermal drug delivery. *Eur. J. Pharm. Biopharm.* **2018**, *128*, 170–178. [[CrossRef](#)] [[PubMed](#)]
34. Vidlářová, L.; Romero, G.B.; Hanuš, J.; Štěpánek, F.; Müller, R.H. Nanocrystals for dermal penetration enhancement - Effect of concentration and underlying mechanisms using curcumin as model. *Eur. J. Pharm. Biopharm.* **2016**, *104*, 216–225. [[CrossRef](#)] [[PubMed](#)]
35. Hecq, J.; Deleers, M.; Fanara, D.; Vranckx, H.; Amighi, K. Preparation and characterization of nanocrystals for solubility and dissolution rate enhancement of nifedipine. *Int. J. Pharm.* **2005**, *299*, 167–177. [[CrossRef](#)]
36. Mauludin, R.; Müller, R.H.; Keck, C.M. Kinetic solubility and dissolution velocity of rutin nanocrystals. *Eur. J. Pharm. Sci.* **2009**, *36*, 502–510. [[CrossRef](#)] [[PubMed](#)]
37. Sun, J.; Wang, F.; Sui, Y.; She, Z.; Zhai, W.; Wang, C.; Deng, Y. Effect of particle size on solubility, dissolution rate, and oral bioavailability: Evaluation using coenzyme Q₁₀ as naked nanocrystals. *Int. J. Nanomedicine* **2012**, *7*, 5733–5744. [[CrossRef](#)]
38. Shegokar, R.; Müller, R.H. Nanocrystals: Industrially feasible multifunctional formulation technology for poorly soluble actives. *Int. J. Pharm.* **2010**, *399*, 129–139. [[CrossRef](#)]
39. Regulation (EC) No 1223/2009 of the European Parliament and of the Council of 30 November 2009 on Cosmetic Products; European Commission: Brussels, Belgium, 2009.
40. Jeong, S.H.; Kim, J.H.; Yi, S.M.; Lee, J.P.; Kim, J.H.; Sohn, K.H.; Park, K.L.; Kim, M.-K.; Son, S.W. Assessment of penetration of quantum dots through in vitro and in vivo human skin using the human skin equivalent model and the tape stripping method. *Biochem. Biophys. Res. Commun.* **2010**, *394*, 612–615. [[CrossRef](#)]
41. Pellett, M.A.; Roberts, M.S.; Hadgraft, J. Supersaturated solutions evaluated with an in vitro stratum corneum tape stripping technique. *Int. J. Pharm.* **1997**, *151*, 91–98. [[CrossRef](#)]
42. Voorhees, P.W. The theory of Ostwald ripening. *J. Stat. Phys.* **1985**, *38*, 231–252. [[CrossRef](#)]

